THE JOURNAL OF PHYSICAL CHEMISTRY A

Article

Conformationally Dynamic #-Conjugation: Probing Structure–Property Relationships of Fluorescent Tris(N-salicylideneaniline)s

Mario C Vieweger, Xuan Jiang, Lim Young-Kwan, Junyong Jo, Dongwhan Lee, and Bogdan Dragnea

J. Phys. Chem. A, **Just Accepted Manuscript** • DOI: 10.1021/jp2079583 • Publication Date (Web): 17 Oct 2011

Conformationally Dynamic π-Conjugation: Probing Structure–Property Relationships of Fluorescent Tris(*N*-salicylideneaniline)s

Mario Vieweger, Xuan Jiang, Young-Kwan Lim, Junyong Jo, Dongwhan Lee*, and Bogdan Dragnea*

Department of Chemistry, Indiana University, 800 East Kirkwood Avenue, Bloomington, Indiana 47405

dongwhan@indiana.edu; dragnea@indiana.edu

ABSTRACT: We recently reported the design and synthesis of a series of conformationally dynamic chromophores that are built on the C_3-symmetric tris(*N*-salicylideneaniline) platform. This system utilizes cooperative structural folding–unfolding motions for fluorescence switching, which is driven by the assembly and disassembly of hydrogen bonds between the rigid core and rotatable peripheral part of the molecule. Here, we report detailed time-resolved spectroscopic studies to investigate the structure–property relationships of a series of functionalized tris(*N*-salicylideneaniline)s. Time-resolved fluorescence decay spectroscopy was applied to determine the main relaxation mechanisms of these π-extended fluorophores, and to address the effects of hydrogen bonding, steric constraints, and extension of the π-conjugation on their relaxation dynamics. Our results agree well with the conformational switching model that was previously suggested from steady-state experiments. Notably, extension of the π-conjugation from peripheral aryl groups resulted in the stabilization of the excited states, as evidenced by longer lifetimes and lower non-radiative decay constants. As a consequence, an increase in the fluorescence quantum yields was observed, which could be explained by the suppression of the torsional motions about the C–N bonds from an overall increase in the quinoid character of the excited states. A combination of time-resolved and steady-state techniques also revealed intermolecular interactions through π–π stacking at higher concentrations, which provide additional de-excitation pathways that become more pronounced in solid samples.

Introduction

An increasing number of charge transporters and light emitters are built with organic molecules.[1] The practical utility of such plastic electronics derives from the ability to manipulate the optical and electronic properties of well-defined synthetic systems by either covalent or non-covalent structural modifications of their π-conjugated backbone.[2–4] Within this context, research elsewhere has investigated the relationship between conformational dynamics and photophysical properties of one-dimensional (1-D) π-conjugation.[5] Specifically, it has been shown that conformational restriction and enforced co-planarity of 1-D conjugation lead to a decrease in the HOMO–LUMO gap and enhancement in fluorescence efficiency.[6]

Studies on the structure–property relationships of two-dimensional (2-D) conjugation should complement such efforts by providing additional data sets to be tested and interpreted using models developed for simpler 1-D systems.[7] For 2-D systems, the added dimensionality of electron delocalization at excited states clearly impacts the photophysical properties of π-conjugation beyond the confinement of linear skeleton.[8] Understandably, directional transfer of excited-state energies in light-harvesting systems has been one of the major driving forces in such research.[3] The shape-persistent nature of the rigid π-conjugation pathways supported by either hyperbranched or ring-fused 2-D structural skeletons play a critical role by reducing conformational disorder and preventing thermal dissipation of energy.[9] Evaluation and elaboration of structure–property relationships in 2-D structural settings, however, require access to structural motifs that allow for facile and systematic modification of relevant geometric and electronic parameters.

We recently reported the synthesis and characterization of a series of C_3-symmetric π-conjugation that utilize cooperative structural folding–unfolding motions for fluorescence switching (Scheme 1).[8,10–15] These fluorophores have three *ortho*-substituted aryl groups that are attached directly to the three-fold symmetric tris(*N*-salicylideneamine) core $\{C_6O_3(CHNH)_3\}$,[16,17] which mimics the *shape* of triphenylene.[18] As shown in Scheme 1, the O–H···O hydrogen bonding contacts between the alcohol groups at the "wingtips" of the aryl rings and the ketone oxygen atoms of the molecular core stabilize the "folded"

conformer **A**. In addition to flattening the entire structure to define an extended π-conjugation, such intramolecular hydrogen-bonding network suppresses internal torsional motions of **A** to make it fluorescent. Loss of such O–H···O contacts results in the "unfolded" and non-emissive conformer **B** (Scheme 1) having freely-rotating C–N bonds. Here, the lack of structure-rigidifying hydrogen bonding interactions facilitates non-radiative decay of the excited states through internal torsional motions. This simple mechanistic model was supported by the loss of fluorescence intensity in the presence of hydrogen-bonding DMSO solvents or F^- anions, which effectively compete with the intramolecular O–H···O hydrogen bonds to unfold the molecule.[10] This fluorescence on–off switching scheme, which is based on the hydrogen bonding between the rotatable perimeter and the rigid core of the fluorophores, was exploited subsequently for a turn-on signaling of fluoride ions in solution,[12] and signal amplification through orientation-dependent fluorescence resonance energy transfer (FRET).[13]

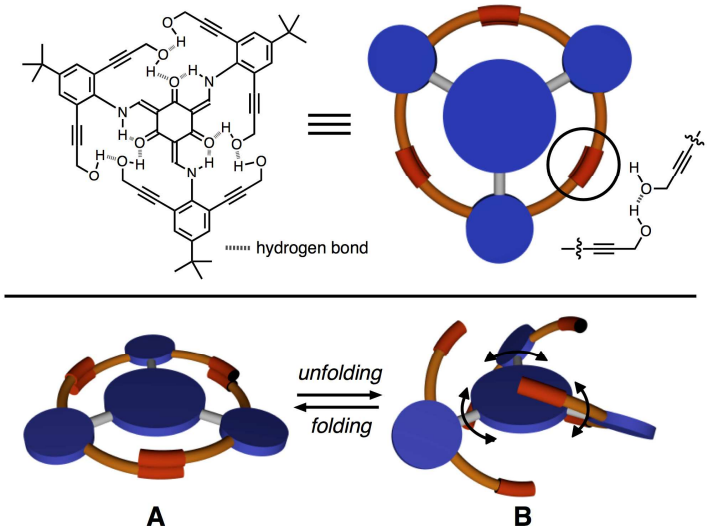

Scheme 1. Chemical structure of a functionalized tris(*N*-salicylideneaniline) and a cartoon-style representation of its "folded" conformation (**A**) through a cyclic array of intramolecular hydrogen bonds. Loss of these key O–H···O–H···O contacts leads to structural "unfolding" (**B**) with freely rotating C–N bonds between the C_3-symmetric molecular core and peripheral aryl groups.

The use of functionalized tris(*N*-salicylideneaniline)s as stimuli-responsive molecular switches and sensors should benefit significantly from (i) maximizing changes in the emission intensity (ΔI) upon

structural folding–unfolding, and (ii) modulating spectral windows of photo-excitation and emission through structural modifications of the π-conjugation. Detailed spectroscopic studies on a homologous set of molecules should thus provide useful structure–property relationships that will guide rational structure design in such directions. Toward this objective, we initiated comparative spectroscopic studies on compounds **1**–**10** listed in Figures 1 and 2.

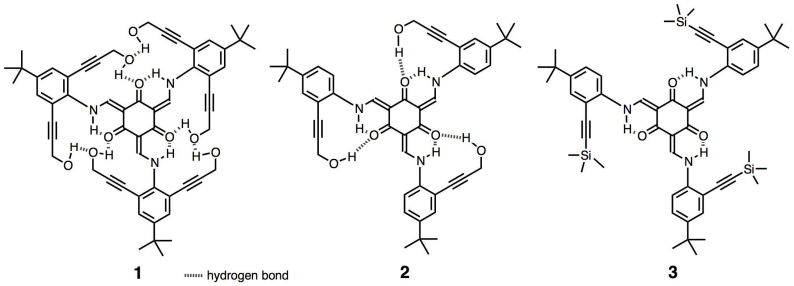

Figure 1. Chemical structures of tris(*N*-salicylideneaniline) derivatives **1**–**3**.

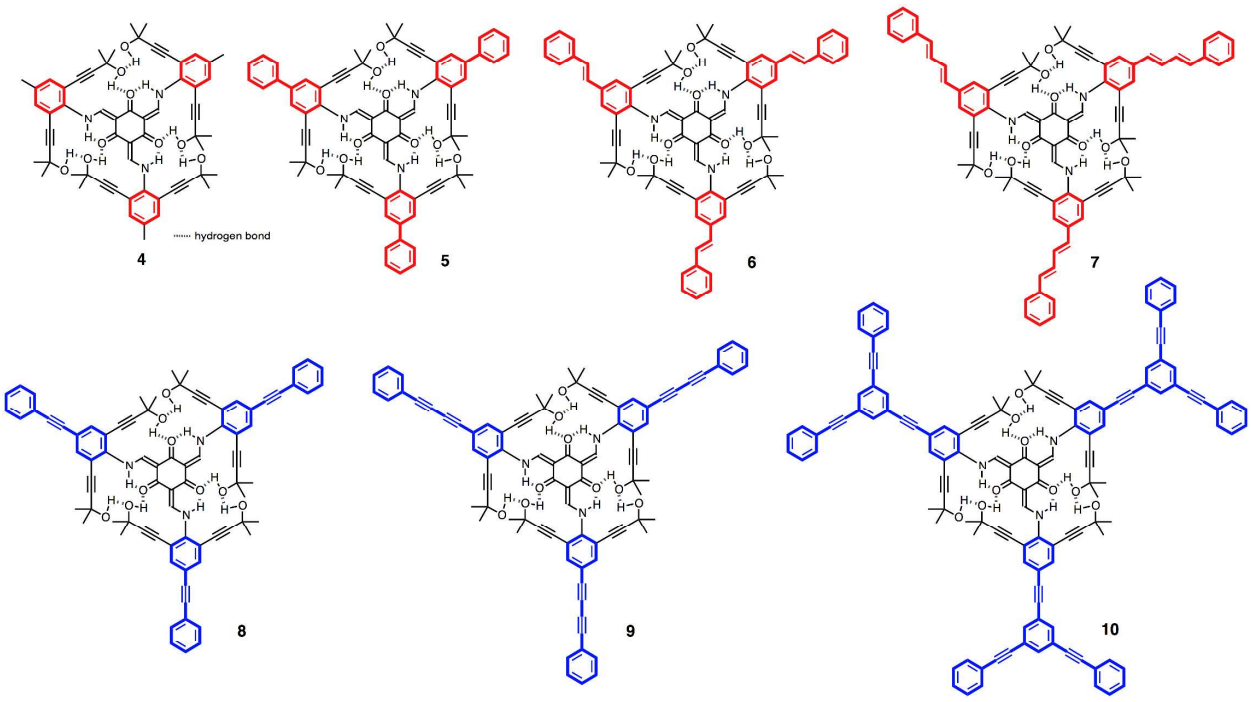

Figure 2. Chemical structures of π-extended tris(*N*-salicylideneaniline) derivatives **4**–**10**.

The series **1**–**3** (Figure 1) were investigated specifically to address the role of hydrogen bonding and steric constraints on the stability of the excited states. The series **4**–**10** (Figure 2) were studied to delineate the effects of extended π-conjugation on both the energy window and efficiency of light emission. We applied time-resolved spectroscopy to determine the origins and kinetics of the main relaxation mechanisms of these functionalized tris(*N*-salicylideneaniline)s **1**–**10**. Individual contributions of these excited-state decay processes on the commonly measured steady-state properties, such as fluorescence spectra and emission quantum yields, were evaluated across the series, the details of which are presented in this work.

Experimental Section

General Considerations. All reagents were obtained from commercial suppliers and used as received unless otherwise noted. Diisopropylamine was degassed by freeze-pump-thaw cycles (× 3) and stored under nitrogen. The compounds 1,3,5-triformylphloroglucinol[16a] and 2-iodo-4-*tert*-butyl-aniline[19] were prepared according to literature procedures. The syntheses of **1**,[10] **2**,[12] and **4**–**10**[11] have previously been reported. All air-sensitive manipulations were carried out under nitrogen atmosphere in an M.Braun glovebox or by standard Schlenk-line techniques.

Physical Measurements. ^{1}H NMR and ^{13}C NMR spectra were recorded on a 400 MHz Varian Inova NMR Spectrometer or a 300 MHz Varian Gemini 2000 NMR spectrometer. Chemical shifts were reported vs. tetramethylsilane and referenced to the residual solvent peaks. High-resolution chemical ionization (CI) and electrospray ionization (ESI) mass spectra were obtained on a Thermo Electron Corporation MAT 95XP-Trap using CH_4 as CI reagent. FT-IR spectra were recorded on a Nicolet 510P FT−IR Spectrometer with EZ OMNIC E.S.P. software. UV–vis spectra were recorded on a Perkin-Elmer Lambda 19 UV/vis/near-IR spectrometer or a Varian Cary 100 Bio UV-Visible Spectrophotometer. Steady-state fluorescence spectra were recorded on a Perkin Elmer LS50B Luminescence Spectrometer or a Photon Technology International QM-4-CW Spectrofluorometer with FeliX32 software. Measurements were performed under temperature control and purging with dry nitrogen for temperatures below 15 °C.

Fluorescence measurements were performed with an excitation at 380 nm, and concentrations were chosen with absorbances below 0.1 to reduce the inner filter effect. The fluorescence spectra were integrated and the quantum yields obtained according to eq. (1) using Coumarin 30 ($Q = 0.67$ in MeCN solution) as a reference:[20,21]

$$Q_f = Q_{st}\left(\frac{Grad_f}{Grad_{st}}\right)\left(\frac{\eta_f^2}{\eta_{st}^2}\right) \quad (1)$$

The indices *f* and *st* stand for the fluorophore and the quantum yield standard (= reference molecule), respectively. *Q* represents the emission quantum yield, *Grad* is the gradient of integrated fluorescence intensity vs. absorbance at λ = 380 nm, and η is the index of refraction of the solvent.

Lifetime Measurements. Samples were excited by a mode-locked Ti:S laser (Mira 900-F, Coherent Inc., CA) with a repetition rate of 76 MHz and a pulse duration of less than 200 fs. In order to allow for two-photon absorption to occur, the 800 nm output was focused onto the sample. Fluorescence photons were detected orthogonal to the incident beam on a fast photomultiplier tube (PMA 165-P, PicoQuant GmbH, Germany), pre-amplified, and collected by time-correlated single photon counting (TCSPC) electronics (TimeHarp200, PicoQuant, GmbH, Germany) for processing (Figure 3).

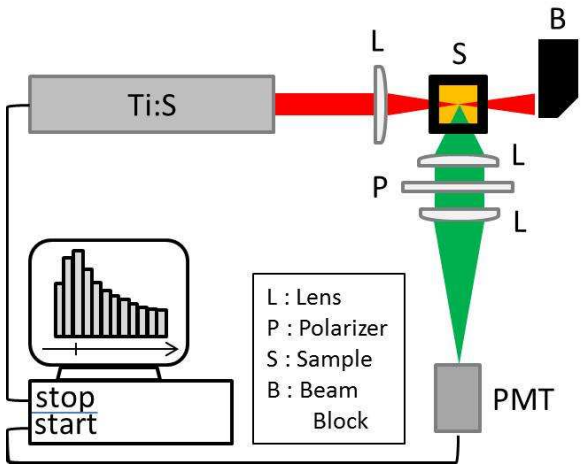

Figure 3. Experimental setup for time-correlated single photon counting (TCSPC).

A short pass filter and a Glan-Taylor polarizer at magic angle position (54.7 °) were placed in the detection path to ensure that only fluorescent photons were detected and to avoid rotational diffusion artifacts. Temperature control was achieved with a FLASH 200 Fluorescence Cuvette Holder (Quantum Northwest Inc., Seattle) under dry-gas purging. The wavelength and bandpass selections were obtained using a H10 VIS monochromator (HORIBA Jobin Yvon Inc., NJ). The monochromator features a holographic grating with a linear dispersion of 1200 g/mm, which corresponds to a bandpass of 8 nm/mm slit width. Due to intensity and concentration considerations, a bandpass of 16 nm was chosen and measurements were obtained at 5 nm intervals throughout the fluorescence spectrum of the sample.

Fluorescence decay curves were fitted to a multi-exponential decay model (eq. 2) using global fluorescence decay data analysis software (FluoFit 4.2, PicoQuant, GmbH, Germany).[22–29] The goodness of the fits was evaluated according to their reduced χ^2-values,[26,27] the normal deviate of the reduced χ^2-value ($Z\chi^2$),[26] the plot of the weighted residuals,[26,30] and the autocorrelation function[26,27] of the weighted residuals. Only the fits with the lowest number of excited-state lifetimes that gave satisfactory fitting results were used for further analysis.

$$I(t) = \sum_{i=1}^{n} \alpha_i e^{\left(-\frac{t}{\tau_i}\right)} \tag{2}$$

where *I(t)* is the recorded intensity at time t, α_i is the pre-exponential factor or amplitude of decay component i, τ_i is the lifetime, and t is the measurement duration.

The lifetimes and their corresponding pre-exponential factors thus obtained were then used to calculate weighing factors for lifetime specific contributions to the average lifetimes and steady-state properties. These weighing factors are the fractional amplitude (a_i) and the fractional intensity (f_i):

$$a_i = \frac{\alpha_i}{\sum_{i=1}^{n} \alpha_i} \tag{3}$$

$$f_i = \frac{\int_0^\infty I_i(t)dt}{\int_0^\infty I(t)dt} = \frac{\alpha_i \tau_i}{\sum_{i=1}^n \alpha_i \tau_i} \quad (4)$$

The fractional amplitude a_i is the fraction of the integral under the decay curve with which component i contributes to the total detected fluorescence intensity ($\sum_{i=1}^n \alpha_i = 1$ and therefore $a_i = \alpha_i$). The fractional intensity f_i takes into account the lifetime and therefore the average duration of the lifetime-specific excitation-emission cycles ($\sum_{i=1}^n f_i = 1$).

The average lifetimes are defined as the sum over the products of weighing factor and lifetime for $i = n$ contributing decay components:

$$\langle \tau \rangle_a = \frac{\sum_{i=1}^n \alpha_i \tau_i}{\sum_{i=1}^n \alpha_i} = \sum_{i=1}^n \alpha_i \tau_i \quad (5)$$

$$\langle \tau \rangle_f = \frac{\sum_{i=1}^n \alpha_i \tau_i^2}{\sum_{i=1}^n \alpha_i \tau_i} = \sum_{i=1}^n f_i \tau_i \quad (6)$$

Consistently, the average lifetimes are referred to as amplitude-averaged ($\langle \tau \rangle_a$) and intensity-averaged ($\langle \tau \rangle_f$). The latter represents the average period of time the chromophore stays in the excited state, while the former turns out to be the parameter of choice for most quantitative analysis due to its relation to the steady-state fluorescence spectrum.[31] For details of decay analysis and lifetime fitting results, see Supporting Information.

4-*tert*-Butyl-2-((trimethylsilyl)ethynyl)aniline. In a glove box, $PdCl_2(PPh_3)_2$ (30 mg, 43 μmol) and CuI (16 mg, 84 μmol) were loaded into a 50-mL tube equipped with a Teflon-lined screw cap. The tube was sealed, removed from the glove box, and placed under nitrogen atmosphere. Portions of 2-iodo-4-*tert*-butylaniline (0.38 g, 1.4 mmol), trimethylsilylacetylene (0.30 g, 3.0 mmol), and a mixture of

$^{i}Pr_2NH$/THF (10 mL, 1:1, v/v) were delivered under nitrogen atmosphere. The reaction mixture was stirred at r.t. for 12 h, and filtered through a pack of Celite. The filtrate was concentrated under reduced pressure, and the residual brown material was purified by flash column chromatography on SiO_2 (hexanes:EtOAc = 10:1, v/v) to afford a yellow oil (0.274 g, 1.12 mmol, 79%). ^{1}H NMR (300 MHz, $CDCl_3$): δ 7.32 (d, J = 1.8 Hz, 1H), 7.16 (dd, J = 8.4, 1.8 Hz, 1H), 6.64 (d, J = 8.4Hz, 1H), 4.10 (br s, 2H), 1.23 (s, 9H), 0.22 (s, 9H). ^{13}C NMR (100 MHz, $CDCl_3$): δ 145.9, 140.5, 128.6, 127.2, 114.0, 107.2, 102.4, 98.9, 33.8, 31.3, 0.14. FT-IR (thin film on NaCl, cm^{-1}): 3477, 3380, 2960, 2903, 2868, 2147, 1726, 119, 1500, 1463, 1408, 1363, 1304, 1278, 1250, 1159, 928, 844, 760, 698, 653, 629, 492. HRMS (CI) calcd for $C_{15}H_{23}NSi$ $[M]^+$ 245.1594, found 245.1593.

2,4,6-Tris((4-*tert*-butyl-2-((trimethylsilyl)ethynyl)phenylamino)methylene)cyclohexane-1,3,5-trione (3). A solution of 1,3,5-triformylphloroglucinol (40 mg, 0.19 mmol) and 4-*tert*-butyl-2-((trimethylsilyl)ethynyl)aniline (0.271 g, 1.10 mmol) in anhydrous EtOH (10 mL) was heated at 90 °C under nitrogen for 12 h. With progress of the reaction, the mixture became heterogeneous. The product was isolated by filtration, washed with EtOH, and dried in vacuo to furnish **3** as a yellow powder (0.15 g, 0.17 mmol, 90%). ^{1}H NMR (400 MHz, $CDCl_3$): δ 13.68 (d, J = 12.9 Hz, 3H), 8.79 (d, J = 12.9 Hz, 3H), 7.52 (d, J = 1.8 Hz, 1H), 7.41 (dd, J = 8.4, 1.8 Hz, 1H), 7.31 (d, J = 8.4Hz, 1H), 1.31 (s, 9H), 0.46 (s, 9H). ^{13}C NMR (100 MHz, $CDCl_3$): δ 185.1, 147.4, 147.1, 139.2, 129.7, 127.3, 113.4, 113.1, 107.6, 102.3, 99.9, 34.5, 31.2, 0.06. FT-IR (thin film on NaCl, cm^{-1}): 2960, 2901, 2868, 2154, 1614, 1594, 1573, 1444, 1347, 1286, 1268, 1239, 1034, 986, 927, 844, 815, 760, 634, 491. HRMS (CI) calcd for $C_{54}H_{69}N_3O_9Si_3$ $[M]^+$ 891.4641, found 891.4624.

Results and Discussion

Conformational Dynamics in Solution. The design of **1**–**3** takes into account variations in the number of hydrogen bonds and the degree of steric constraints, which should impact conformational dynamics of the molecules in solution (Scheme 1). As we reported previously,[10,12] both **1** and **2** have symmetry-reinforced $O_{hydroxyl}$–H···$O_{hydroxyl}$–H···O_{keto} (for **1**) or $O_{hydroxyl}$–H···O_{keto} (for **2**) hydrogen bonding

interactions between the peripheral aryl rings and the tris(*N*-salicylideneaniline) core (Figure 1), which function as a conformational lock to effectively flatten the molecule (Scheme 1). A close comparison of the X-ray structures reveals a larger dihedral angle (see Figure 4) for **1** (20.9˚) relative to **2** (10.9–11.9˚), which apparently reflects an increased steric congestion between the ethynyl-extended wing-tip groups in **1** that are brought in close proximity upon structural folding (Scheme 1). For comparative studies, compound **3** was prepared as a reference system that does not have any hydrogen bonds between the core and peripheral aromatics.

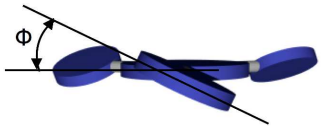

Figure 4. Deviation of the peripheral aryl rings from the tris(*N*-salicylideneanilinle) core as measured by the dihedral angle ϕ.

In CH_2Cl_2 at 25 °C, **2** displays intense (ε = 93000 M^{-1} cm^{-1}) visible absorptions at $\lambda_{max,abs}$ = 419 and 440 nm (Figure 5), which are slightly red-shifted with respect to those of **1** ($\lambda_{max,abs}$ = 414 and 432 nm). Following excitation at λ = 340 nm, **2** emits at $\lambda_{max,em}$ = 458 nm with a small Stokes shift (Δλ = 18 nm), which is smaller than that of **1** (Δλ =30 nm) and presumably reflects the more rigid molecular structure. In support of this notion, the fluorescence quantum yield (= Q_f) of **2** is 9.7%, which is significantly higher than that (Q_f = 4.2%) of **1** under similar conditions. While **3** shows comparable absorption and emission features to **2**, its fluorescence quantum yield of Q_f = 1.6% is more than six-times lower than that of **2**.

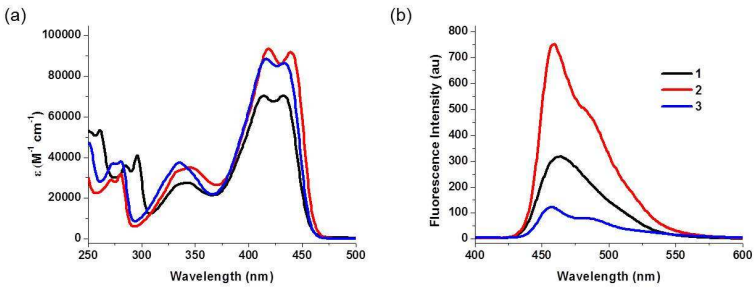

Figure 5. (a) Electronic absorption and (b) emission spectra of **1**–**3** in CH_2Cl_2 at T = 25 ˚C.

Our initial experiments thus targeted a better understanding of the relationship between molecular structure, optical properties, and dynamic behavior of **1**–**3** in solution. For this purpose, time-resolved fluorescence spectroscopy was applied. As described by eqs 7 and 8, Q_f corresponds to the probability that the excited state is deactivated by a radiative rather than a non-radiative pathway, with rate constants of k_r and k_{nr}, respectively. This relationship allows for a quantitative analysis of the competing processes and the stability of the excited states of the molecules.[32,33] While most chromophores have only one radiative pathway, several competing non-radiative pathways may exist. In order to account for such possibilities, k_{nr} is defined as the sum of the rate constants of all non-radiative decay pathways involved.

$$Q_f = \frac{k_r}{k_r + k_{nr}} = \tau \cdot k_r \tag{7}$$

$$\tau = \frac{1}{k_r + k_{nr}} \tag{8}$$

Using the instrument setups (Figure 3) and procedures described in the Experimental Section, we recorded and analyzed fluorescence decay of **1**–**3** by TCSPC. While fitting with two exponential decay components provided reasonable results for **3** (Figure 6c), an additional third decay component was required to fit the lifetime decay curves of **1** and **2** (Figures 6a and 6b).

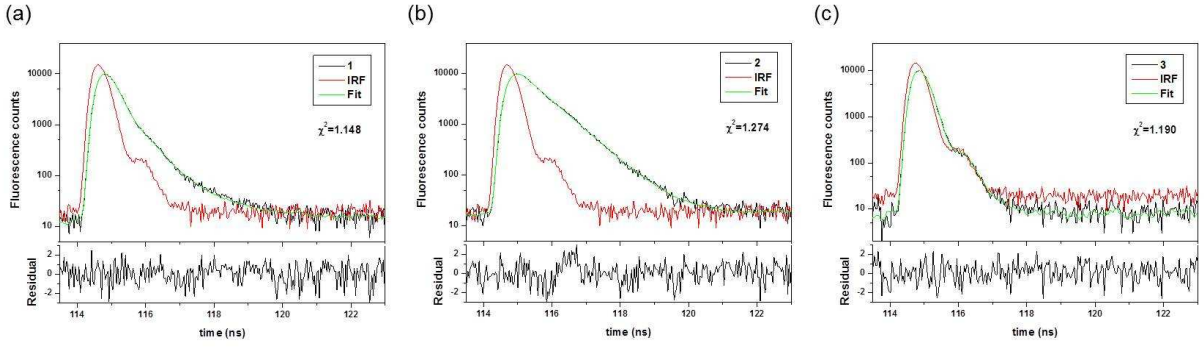

Figure 6. Fluorescence decay profile and instrument response function (IRF) for (a) **1**, (b) **2**, and (c) **3** in CH_2Cl_2 at T = 20 ˚C. The quality of the fits is indicated by the low χ^2 values and the random distribution of weighted residuals, which are shown below for each plot.

A summary of the individual lifetimes and fractional intensities obtained from time-resolved studies is provided in Table 1. Here, lifetimes were assigned to three domains, τ_1 (0.1–0.3 ns), τ_2 (0.45–0.8 ns) and τ_3 (1.4–1.9 ns), the physical meaning of which became our immediate interest. According to the fractional intensities (f_1–f_3), compound **1** has significant contributions from both τ_1 (79%) and τ_2 (18%), and a trace amount of τ_3 (3%). On the other hand, **2** shows small amounts of τ_1 (9%) and τ_3 (5%) components but a significant contribution from τ_2 (86%). In **3,** τ_1 (99%) prevails and τ_3 could not be detected within the sensitivity of the setup.

Table 1. Lifetime measurements of **1**–**3** from single deconvolution fitting.

Compound	τ_1 (ns)	τ_2 (ns)	τ_3 (ns)	f_1	f_2	f_3	$<\tau>_{int}$ (ns)
1	0.209 ± 0.002	0.592 ± 0.017	1.84 ± 0.13	0.786 ± 0.003	0.185 ± 0.002	0.029 ± 0.002	0.327 ± 0.004
2	0.295 ± 0.003	0.719 ± 0.001	1.74 ± 0.04	0.092 ± 0.013	0.860 ± 0.012	0.048 ± 0.001	0.729 ± 0.012
3	0.110 ± 0.002	0.678 ± 0.099		0.988 ± 0.002	0.012 ± 0.002		0.116 ± 0.002

The results from the deconvolutions were then used to calculate amplitude-averaged lifetimes, as well as radiative and non-radiative rate constants listed in Table 2. While no significant differences were observed in the radiative rate constants for **2** (0.149 ns^{-1}) and **3** (0.144 ns^{-1}), which share an essentially identical π-skeleton, **1** having an additional ethynyl unit on each aniline fragment shows a slightly higher k_r of 0.241 ns^{-1}. In contrast to the radiative rate constants, the non-radiative rate constants differ significantly across the series **1**–**3**. While the range of radiative rate constants spans less than a factor of two, the lack of hydrogen bonding results in a more than six-fold increase in the non-radiative rate constants when a comparison is made between **2** and **3**.

Table 2. Radiative and non-radiative decay constants of **1**–**3** at T = 20 ˚C.

Compound	k_{nr} (ns^{-1})	k_r (ns^{-1})	Q_f	$<\tau>_{amp}$ (ns)	Stokes shift (nm)
1	3.85	0.241	0.059	0.245 ± 0.002	30
2	1.39	0.149	0.097	0.651 ± 0.006	18
3	8.88	0.144	0.016	0.111 ± 0.002	23

A significantly decreased fluorescence quantum yield of **3** is thus a consequence of an increase in k_{nr}, rather than a decrease in k_r. This finding quantitatively substantiates the intuitive fluorescence switching model shown in Scheme 1, in which the loss of structural rigidity opens additional non-radiative channels for de-excitation of **B**, in a situation similar to **3**. Consistent with this model, the smallest k_{nr} of 1.39 ns^{-1} in the series (Table 2) is associated with **2** having the highest Q_f of 9.7%. In order to better understand the nature of non-radiative decay pathways that dictate the emissive properties of these molecules, we decided to investigate the origins of the individual lifetime components of **1**–**3**.

Intermolecular Interactions in Solution. A dynamic interconversion between the planar **A** and non-planar **B** conformer (Scheme 1) was previously investigated by variable-temperature (VT) ^{1}H NMR spectroscopy on solution samples.[15] While most fluorophores operate by a single emitting state, the involvement of at least two different conformations of tris(*N*-salicylideneaniline)s in solution immediately raises the question of how many emissive species actually contribute to the experimentally observed fluorescence spectra. In order to address this point, we monitored the wavelength dependence of the decay response across the entire emission spectrum. Using the steady-state emission intensity of the sample, $F^{ss}(\lambda)$, as a reference, spectra associated with the individual fluorescence decay lifetimes ($DAS(\lambda, \tau_i)$), were reconstructed using eq 9:[34]

$$DAS(\lambda,\tau_i) = \frac{\alpha_i(\lambda)}{\sum \alpha_i(\lambda)\tau_i} F^{ss}(\lambda) \tag{9}$$

In order to collect a sufficient amount of photons (10000 cts) in a reasonable amount of time (< 10 min), a compromise was needed between the resolution and measurement time. A total of 18 measurements were thus taken in increments of 5 nm with a bandwidth of 8 nm. The decay profiles thus obtained were analyzed globally, the results of which are displayed in Figure 7: the steady-state fluorescence spectra (F^{ss}) are in black; the decay-associated spectra are in red (τ_1), green (τ_2), and blue (τ_3).

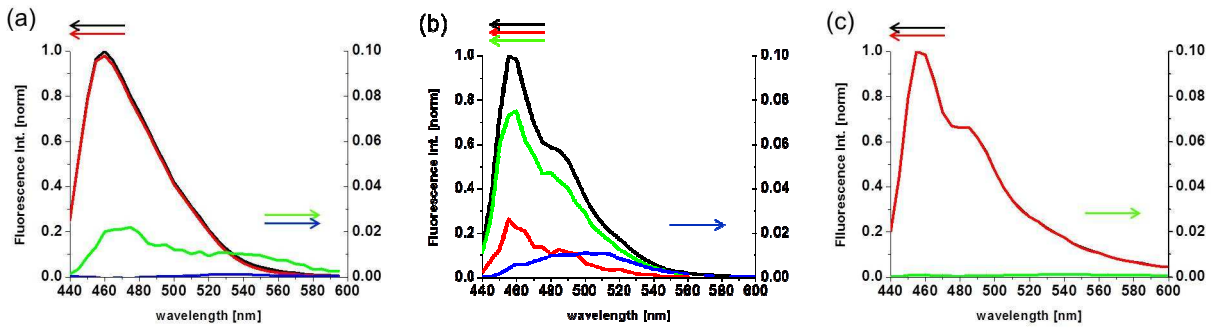

Figure 7. Steady-state fluorescence spectra (black) of (a) **1**, (b) **2**, and (c) **3**, comprised of contributions from DAS of different lifetimes τ_1 (red), τ_2 (green), and τ_3 (blue) in CH_2Cl_2 at $T = 25$ °C.

Despite limitations in the spectral resolution of the current set up, the decay-associated spectra (*DAS*) clearly revealed the emergence of two emission maxima for **1** and **2**. The main emission with peak intensity at $\lambda = 456–464$ nm corresponds to τ_1 and τ_2, whereas the emission of τ_3 appears red-shifted at $\lambda =$ 490–540 nm. The emission maxima of τ_1 and τ_2 are within two data points of the DAS, which makes it less straightforward to interpret whether they originate from distinctive species or minor changes in the conformation of the same chromophore. The emission associated with the τ_3 component, however, is markedly red-shifted from those of τ_1 and τ_2 (see Figure 7b, for example), and is associated with the longest lifetime (Table 1). These properties suggest a more extended electronic structure that typically evolves from intermolecular interactions of π-conjugated molecules in solution.[35]

If intermolecular π–π interaction is indeed responsible for the emitting species with τ_3, its solution population would show concentration dependence. We thus carried out TCSPC experiments on solution samples with a concentration range of 50–500 μM in order to examine the involvement of such solution "aggregates". In order to ensure that the changes in fractional intensities directly reflect the changes in the composition of the excited state, measurements were preformed over the same amount of fluorescent photons. For **1** and **2**, the red-shifted component with the lifetime τ_3 shows an increase in fractional intensities towards higher concentrations (Figure 8). This increase amounts to 1.9 ± 0.7% for **1** and 10.9 ± 0.9% for **2**. In contrast, no significant changes in the intensities could be detected for **3** (0.4 ± 0.2%). This

concentration dependence of the fractional intensities suggests that the red-shifts in the DAS are due to intermolecular interactions that lead to aggregation in solution, presumably via stacking of rigid flat molecules assisted by O–H···O contacts between individual molecules (vide infra). These findings are in accordance with the observation of intermolecular hydrogen bonds in the X-ray structure of **2**,[12] which might occur for molecules in solution. The lack of such hydrogen bonding capabilities also explains why no stacking (and therefore no τ_3 component) could be detected for **3**.

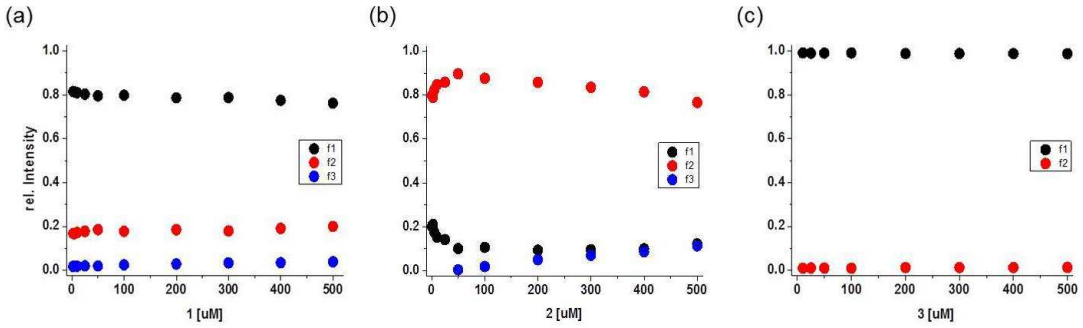

Figure 8. Concentration-dependent changes in the relative intensities (f_1, f_2, and f_3) of lifetime components (τ_1, τ_2, and τ_3) plotted for (a) **1** (b) **2**, and (c) **3**.

In order to correlate the dynamics in solution with molecular structures and to determine if such stacking interactions occur for molecules in the ground state or in the excited state, solid-state samples were prepared by dropcasting **1** or **2** on glass substrates. TCSPC experiments on these samples revealed good fits for two decay components for **1** and **2** (Table 3). The lifetimes are on the order of 0.45–0.56 ns and 1.3–1.9 ns, which overlap fairly well with the lifetimes τ_2 and τ_3 of solution samples. The corresponding fractional intensities show a significant increase in the longest decay component with 26.8 ± 5.8% for **1** and 40.2 ± 2.7% for **2**, compared to 1.9 ± 0.7% and 10.9 ± 0.9% obtained for the corresponding solution samples at the high concentration end (500 μM). The third, shortest lifetime component could not be detected, which may be due to the suppression of non-radiative decay pathways due to a dense packing of the molecules within the solid film.

Table 3. Lifetime measurements of solid samples of **1** and **2**.

Compound	τ_2 (ns)	τ_3 (ns)	f_2	f_3	$<\tau>_{int}$
1	0.459 ± 0.006	1.31 ± 0.02	0.732 ± 0.058	0.268 ± 0.058	0.686 ± 0.049
2	0.555 ± 0.009	1.83 ± 0.03	0.598 ± 0.027	0.402 ± 0.027	1.066 ± 0.034

A higher degree of stacking found for **2** (40%) relative to **1** (27%) in the solid state, as deduced from the fractional intensities (Table 3), indicates that its molecular geometry prefers intermolecular interactions. One structural parameter to evaluate the overall planarity of the molecule, as well as the degree of conjugation, is the dihedral angle ϕ between peripheral aryl rings and the core unit (Figure 4). Steric interactions between two neighboring propargyl alcohol groups, three pairs in total (Scheme 1 and Figure 1), result in a relatively large dihedral angle of 20.9 ° in **1**.[10] The absence of such steric congestion allows **2** to fully relax and orient more properly in the plane of the π-system, which results in smaller dihedral angles of 10.9–11.9 °.[12] This planar arrangement presumably allows for a more favorable intermolecular interaction, which is reflected in the higher fractional intensity of the τ_3 component in **2**.

The solution dynamics leading to aggregation was probed independently by concentration-dependent ^{1}H NMR spectroscopy. The chemical shifts of the O–H protons in **1** and **2** were monitored in $CDCl_3$ over the concentration range of 1–50 mM at 25 ºC. As shown in Figure 9, the O–H proton resonances of **1** show negligible change from 5.24 to 5.25 ppm. The chemical shifts of other protons, such as those associated with the enamine N–H, vinyl, and aromatic C–H protons also remain essentially unchanged. In contrast, the O–H protons of **2** show significant downfield shift from 5.20 to 5.49 ppm with an increase in concentration (Figure 9a), whereas other protons shift to upfield. For example, the N–H protons shift from 13.95 to 13.55 ppm and the C–H protons from 8.59 to 8.80 (Figures 9b and 9c). These observations suggest that an intermolecular association is indeed occurring for **2** in solution, leading to stacking and aggregation at higher concentrations.

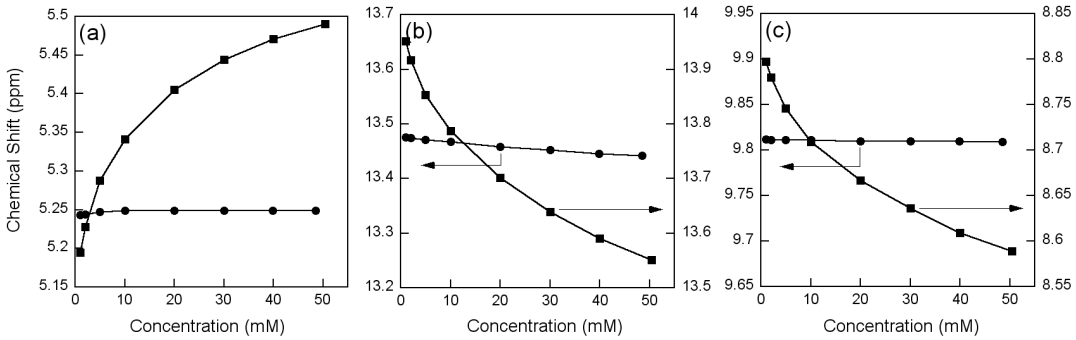

Figure 9. Concentration-dependent (1–50 mM) changes in the (a) $O_{hydroxyl}$–H, (b) $N_{enamine}$–H, and (c) C_{vinyl}–H proton resonances of **1** (in circles) and **2** (in squares) in $CDCl_3$ at T = 25 ºC.

In sum, the time-dependent spectral decay and the concentration dependence of TCSPC and ^{1}H NMR data are consistent with the existence of aggregation in solution, which results in a red-shifted emission and elongated lifetime of τ_3. We thus conclude that τ_3 results from a concentration-dependent intermolecular process rather than conformational switching of discrete molecular species (Scheme 1).

Photophysical Consequences of Hydrogen Bonding and Steric Constraints. Findings described in the previous section suggest that contribution of τ_3 can be suppressed by lowering sample concentrations. Under such conditions, the excited states associated with τ_1 and τ_2 could be studied with minimal complications from intermolecular processes. As the DAS did not allow a clear distinction of the components associated with τ_1 and τ_2, the nature of the de-excitation pathways was explored by studying their temperature dependence. Previous time-resolved studies on simple *N*-salicylideneaniline derivatives identified two decay components with lifetimes that are similar to those observed for **1**–**3**.[36] These lifetimes were explained by invoking an isomerization between the *cis*-keto* and *twist*-keto* form of the molecule in the excited state. The feasibility of similar processes at the tris(*N*-salicylideneaniline) core prompted us to investigate the effects of temperature on the fractional intensities of the lifetime components. Subsequent measurements were thus conducted for solution samples of **1**–**3** (25 μM) in $CHCl_3$ from –25 to +50 ˚C (Figure 10).

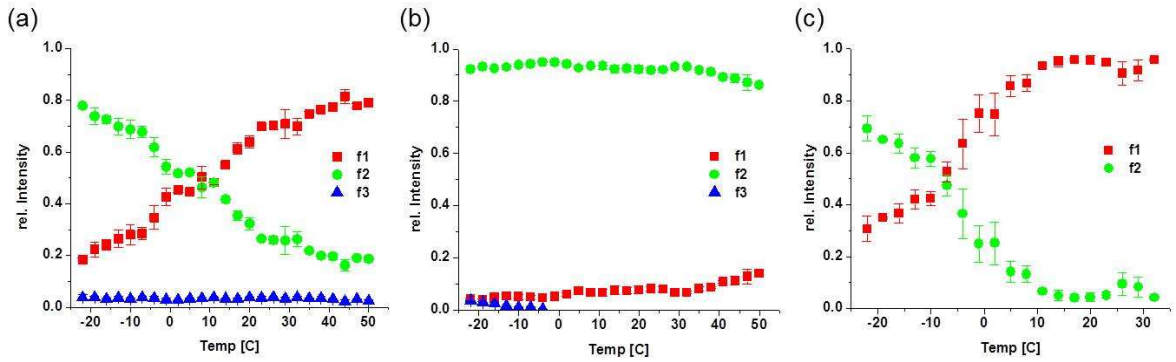

Figure 10. Temperature-dependent changes in the fractional intensities of (a) **1**, (b) **2**, and (c) **3**.

As shown in Figure 10b, the composition of the excited state hardly changes for **2** (85–95% of τ_2) within the temperature range of –25 to +50 ˚C. In contrast, **3** shows an "inversion" in the fractional intensities as a function of temperature (Figure 10c), which results in the decrease of f_2 from ca 70% at –25 ˚C to < 10% above 10 ˚C with concomitant increase of f_1. Under similar conditions, **1** also shows a depletion of the state associated with τ_2 with increasing temperature (from 80% at –25 ˚C to 20% at 50 ˚C), although it slopes less steeply and still contributes significantly (50%) to the excited state at 10 ˚C (Figure 10a). At low temperatures, the state associated with the lifetime τ_2 thus becomes dominant for all three systems, and shows the trend of $f_2(\mathbf{2}) > f_2(\mathbf{1}) > f_2(\mathbf{3})$.

The fractional intensities plotted in Figure 10 show the average population of the excited states associated with individual lifetimes. As the lifetimes change with temperature due to the activation barriers of non-radiative relaxations, so do the populations of the excited states. The nature of the relaxation mechanisms, along with their activation barriers and dependence on temperature, influences the rate at which the population of the excited states changes. The competition between the radiative and non-radiative processes for the relaxation of the molecule results in a lower fluorescence efficiency at a higher temperature and vice versa.

In order to determine whether the inversion in the fractional intensities for **1** and **3** as a function of temperature (Figures 10a and 10c) originates from an inversion in the populations of the excited states or two independent processes with very different temperature dependences, an absolute measurement was

needed. For this purpose, the fractional amplitudes and the steady-state emission quantum yields were used to calculate the lifetime-associated contributions to the total fluorescence quantum yield (eqs 3 and 7). The fractional amplitudes represent the relative contribution that the individual lifetimes have on the total amount of photons recorded. This dependence on the total fluorescence intensity allows calculation of the contribution of individual lifetimes to the emission quantum yield of the molecules. An absolute measure of the components contributing to the steady-state fluorescence is shown in Figure 11, which compares fractional amplitudes of individual lifetimes relative to the total amount of photons recorded.

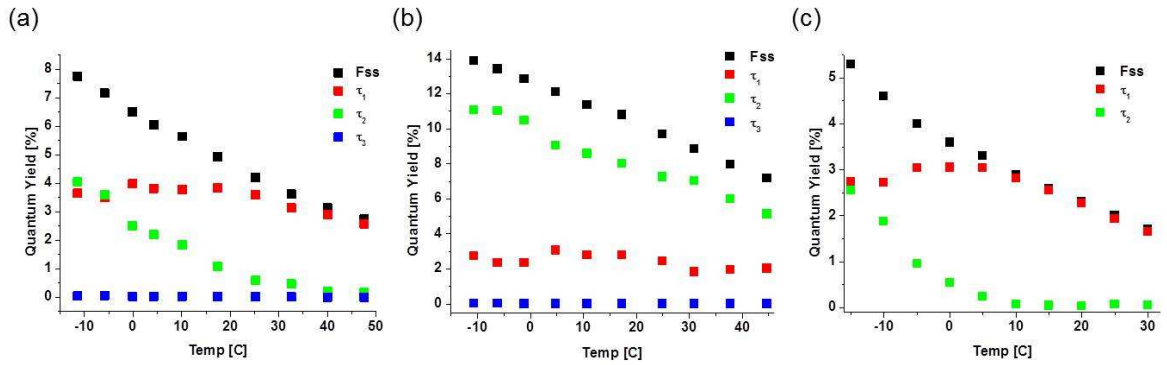

Figure 11. Lifetime-associated contributions of the decay components to the total emission quantum yield of (a) **1**, (b) **2**, and (c) **3** as a function of temperature.

The lifetime dependence of the emission quantum yields plotted in Figure 11 shows the influence that the composition of the excited state has on the fluorescence spectra. Overall, the quantum yields decrease with increasing temperature. This is a typical behavior, which reflects higher rate constants of non-radiative decay at elevated temperatures. As shown in Figure 11, both τ_1 and τ_2 contribute significantly to the total quantum yield at low temperatures. At –10 ˚C, they contribute about equally in the case of **1** and **3**, whereas τ_1 contributes four times as much to the fluorescence intensity of **2** as τ_2. Toward the high temperature end, however, τ_2 loses its contribution. For **1** and **3**, the contribution from τ_1 remains quite steady until it reaches a "critical temperature", beyond which it starts to decrease as well. This critical temperature is 20–25 ˚C for **1**, and 5–10 ˚C for **3**.

According to our analysis of Figure 11, the steady-state emission quantum yields of tris(*N*-salicylideneaniline)s are dictated by an interplay between two different decay components that have significant temperature dependence. The low temperature range below the critical temperature (vide supra) is dominated by τ_2, where contributions from τ_1 remain fairly constant. On the other hand, the high temperature range above the critical temperature is dominated by τ_1, where τ_2 has essentially vanished. For **2**, the critical temperature across which this switching occurs seems to lie above the experimentally accessible temperature window. This might be the reason that τ_2 still has significant contribution to the emission at $T = 50$ ˚C (Figure 11b).

The temperature dependence of the fluorescence lifetime (Figure 10) and the contribution of different decay components to the overall emission quantum yields (Figure 11) suggest that non-radiative decay pathways are available for the excited-state associated with τ_2. The contributions of τ_2 across the series **1**–**3** also concur with the steady-state fluorescence efficiency, which follows the trend of **2** > **1** > **3**. The molecular basis of this non-radiative decay was previously postulated to be structural unfolding through loss of hydrogen bonds (Scheme 1) and thermal relaxation of the excited-state through internal torsional motions. An intriguing observation from Figure 11 is an essentially constant (ca 3%) contribution of the τ_1 component to the emission quantum yields of **1**–**3**, which implicates that this de-excitation pathway is not influenced by hydrogen bonding or steric constraints associated with peripheral aryl groups. It is therefore most likely related to processes occurring at the $\{C_6O_3(CHNH)_3\}$ core, such as a *cis*-keto* to *twist*-keto* isomerization of the *N*-salicylideneaniline fragments.[36] The detailed molecular mechanism responsible for this phenomenon is yet to be elucidated.

Temperature-dependent studies described in this section confirmed that τ_2 is the main relaxation process, which is also responsible for the structure-dependent changes in the fluorescence quantum yields observed for **1**–**3**. The dependence of τ_2 on hydrogen bonding and steric constraints further suggests that the emission efficiency of tris(*N*-salicylideneaniline) fluorophores should be enhanced by suppressing bond twisting about the C_{aryl}–$N_{enamine}$ bonds. One synthetic approach to achieve this goal is installing π-conjugated chemical functionalites at the *para*-positions of the aryl groups so that the excited state could

readily acquire quinoid character with higher rotational barrier of the C_{aryl}–$N_{enamine}$ linkages.[37,38] The following section describes structure–property relationships of such π-extended tris(*N*-salicylideneaniline)s investigated by time-resolved spectroscopic techniques.

Photophysical Consequences of Extending π-Conjugation. The TCSPC studies on **1**–**3** have established that molecules sharing an essentially identical tris(*N*-salicylideneaniline) core have similar k_r values but different k_{nr} parameters (Table 2), which collectively result in markedly different fluorescence emission efficiencies. In order to test the general applicability of this model, we investigated the structure–property relationships of tris(*N*-salicylideneaniline)s **5**–**10** having radially disposed π-conjugations that are extended from the C_3-symmetric core of the parent system **4** (Figure 2). Across the series **4**–**10**, an identical set of structure-rigidifying hydrogen-bonding network is maintained so that our research focus can be placed on the effects of extended π-conjugation on the emitting states.

As we previously reported,[11] compounds **4**–**10** show intense ($\varepsilon > 75000$ $M^{-1}cm^{-1}$) longer wavelength ($\lambda_{abs,max}$ = 415–475 nm) absorptions and blue emissions ($\lambda_{em,max}$ = 453–480 nm). Relatively small Stokes shifts ($\Delta\lambda$ = 24–35 nm) displayed by these molecules are consistent with the rigid nature of their extended π-system and small structural rearrangements upon photoexcitation and de-excitation.[32,33,39] In general, compounds **5**–**10** having extended π-conjugation show red-shifted bands in both absorption and emission relative to those of the reference system **4**.[11] This trend apparently has its origin in the decrease of the HOMO–LUMO gaps by an effective expansion of the π-conjugation, as can be deduced from their chemical structures.

The emission efficiency of tris(*N*-salicylideneaniline)s also depends on peripheral π-extension (Table 4). Compared with the benchmark molecule **4** (Q_f = 5.3%), the fluorescence quantum yields of ethynylene-extended **8** (Q_f = 13%) and **9** (Q_f = 19%) show ca two-fold and four-fold enhancement, respectively. Installation of additional ethynylphenyl branches as in **10**, however, decreased the emission efficiency to Q_f = 12%. A similar trend was observed along the series **4** → **6** → **7**, with an initial enhancement (Q_f = 16% for **6**) followed by a decrease (Q_f = 12% for **7**) with increasing conjugation.

According to eq 7, an increase in Q_f results either from a longer lifetime or a larger radiative decay rate k_r. We thus measured fluorescence decay profiles to track the origins of such behavior.

Table 4. Lifetime and decay rate constants of photo-excited **4**–**10** in $CHCl_3$ at 25 ˚C.

Compound	τ_1 (ns)	τ_2 (ns)	τ_3 (ns)	a_1	a_2	a_3	$<\tau>_{amp}$ (ns)	Q_f	k_{nr} (ns^{-1})	k_r (ns^{-1})
4	0.198	0.364		0.559	0.441		0.218	0.053	4.34	0.243
5	0.186	0.559		0.163	0.837		0.403	0.12	2.18	0.298
6	0.220	0.896		0.130	0.870		0.629	0.16	1.34	0.254
7	0.281	1.06		0.156	0.844		0.674	0.12	1.31	0.178
8	0.206	0.661		0.147	0.853		0.478	0.13	1.82	0.272
9	0.220	0.760		0.156	0.845		0.572	0.19	1.42	0.332
10	0.309	0.962	2.68	0.236	0.720	0.045	0.610	0.12	1.44	0.197

In order to suppress potential aggregation in solution, time-resolved experiments were performed on samples at low concentrations. With the exception of **10**, the emission from π-extended tris(*N*-salicylideneaniline)s could be fitted with two decay components (Table 4), which are of the same order as τ_1 and τ_2 in **1**–**3**. In general, the lifetime tends to increase with extension of the peripheral π-conjugation, with 0.90–1.06 ns and 0.66–0.96 ns for τ_2 in the vinylene- and ethynylene-extended series, respectively, compared with 0.36 ns for the reference molecule **4**. The amplitudes also show an almost two-fold increase in the contribution of τ_2 to the fluorescence spectrum, with 84–87% in **5**–**9** relative to 44% in **4**. These findings suggest that the increase in the emission quantum yields might be due to an enhanced conformational stability of the excited states of π-extended molecules which leads to longer lifetime.

We subsequently determined radiative and non-radiative decay rate constants of **4**–**10** and compared with those of **1**–**3**. As anticipated from their essentially superimposable π-conjugation, **4** has a k_r value similar to that of **1** and only a slightly higher k_{nr} value. The π-extended molecules **5**–**10** show comparable radiative decay rate constants of k_r = 0.172–0.332 ns^{-1}, which decrease slightly with extension of the π-conjugation as shown in Figure 12. On the other hand, a large decrease in the non-radiative decay constant k_{nr} was observed with increasing π-conjugation (Figure 12).

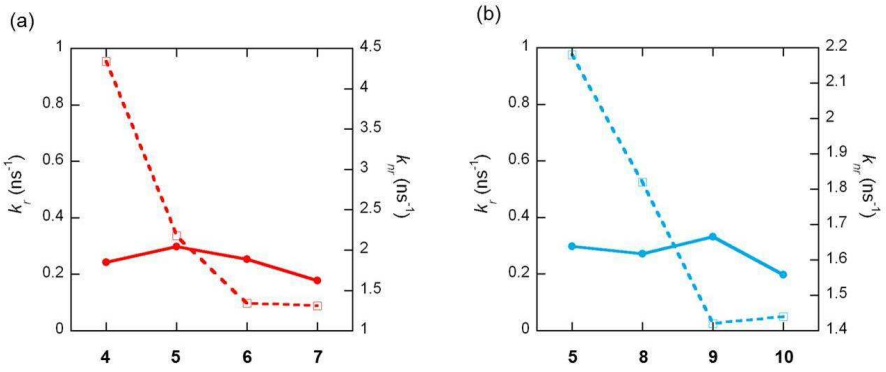

Figure 12. Structure-dependent changes in the k_r (solid lines) and k_{nr} (dashed lines).

Since the torsional motions of aryl rings surrounding the tris(*N*-salicylideneamine) $\{C_6O_3(CHNH)_3\}$ core constitute the main non-radiative decay pathway (Scheme 1), a decrease in k_{nr} with elongated π-conjugation presumably reflects suppressed C_{aryl}–$N_{enamine}$ bond twisting motions resulting from an increased contribution of the quinoid character.[37,38,40] Therefore, a net enhancement in fluorescence quantum yield observed in π-extended tris(*N*-salicylideneaniline)s is not so much from an increase in k_r as from a decrease in k_{nr}. We note, however, that the k_{nr} value essentially levels off at certain points (see changes in k_{nr} upon moving from **6** to **7** in Figure 12a; also from **9** to **10** in Figure 12b), and further structural extension beyond these points have an adverse effect on the emission efficiency since k_r drops slightly while k_{nr} remains essentially constant.

Summary and outlook

We have investigated structure–property relationships of a series of dynamic fluorophores that are built around a C_3-symmetric tris(*N*-salicylideneaniline) core. In solution, these molecules undergo reversible switching motions that interconvert the emissive *folded* and the non-emissive *unfolded* conformer. In order to address the role of hydrogen bonds and steric constraints in this process, a combination of time-resolved and steady-state studies were applied on model systems **1**–**3**. Our concentration- and temperature-dependent TCSPC studies have established (i) good correlation between non-radiative decay rate and fluorescence quantum yield, (ii) contribution of three distinct decay

components τ_1, τ_2, and τ_3 in the de-excitation process. While the structure-independent and temperature-insensitive τ_1 component has a constant contribution to the total quantum yield, the main relaxation process τ_2 changes dramatically as a function of temperature and depends strongly on the presence of hydrogen bonding and steric interactions of peripheral aryl groups involved in conformational switching. In addition, the concentration-dependent τ_3 component implicated interchromophore interactions at higher concentrations, which was independently confirmed by ^{1}H-NMR studies.

Installation of either vinylene- or ethynylene-bridged π-conjugations onto the three-fold symmetric core of these molecules resulted in red-shifts in absorption and emission spectra, along with enhanced emission quantum yields. Fluorescence decay measurements on these π-extended tris(*N*-salicylideneaniline)s **5**–**10** revealed two main decay lifetimes as in simpler systems **1**–**4**. Extension of the π-conjugation apparently results in more stable excited-states due to a decrease in the non-radiative decay rate while the radiative decay rate remains essentially constant across the series.

Prevailing paradigms in π-conjugated organic molecules focus primarily on strategies to rigidify the structural backbone to promote intimate electronic communication between neighboring units. Challenging this "static" view, we have devised chemically intuitive and operationally simple means to trigger-bond twisting motions between neighboring π-fragments, which translate directly to changes in emission properties of tris(*N*-salicylideneaniline)s. Findings described in this work have significantly enhanced our fundamental understanding of the de-excitation pathways of these *conformationally dynamic fluorophores*, and laid a solid groundwork for their rational structural evolution for potential applications in light-harvesting, chemical sensing, and molecular switching.

Acknowledgments. This work was supported by the National Science Foundation (CAREER CHE 0547251) and the U.S. Army Research Office (W911NF-07-1-0533). We further acknowledge support from the National Institutes of Health (grant GM081029) and the Indiana METACyt Initiative of Indiana University, funded in part through a major grant from the Lilly Endowment, Inc. M. C. V. is grateful for a College of Arts and Sciences Dissertation Year Research Fellowship from Indiana University.

Supporting Information Available. Comparison of decay analysis, lifetime fitting results for decay-associated spectra, lifetime fitting results for concentration dependence, lifetime fitting results for temperature dependence, and lifetime fitting results for temperature dependent lifetime-associated contributions to the quantum yields of **1**–**3**. This material is available free of charge via the Internet at http://pubs.acs.org.

References

(1) (a) *Electronic Materials: The Oligomer Approach*; Müllen, K.; Wegner, G., Eds.; Wiley–VCH: New York, 1998. (b) Roth, S.; Carroll, D. *One-Dimensional Metals*; Wiley-VCH: Weinheim, 2004. (c) *Functional Molecular Nanostructures*; Schlüter, A. D., Ed.; Springer: Berlin, 2005. (d) *Organic Electronics*; Klauk, H., Ed.; Wiley-VCH: Weinheim, 2006. (e) *Functional Organic Materials*; Müller, T. J. J.; Bunz, U. H. F., Eds.; Wiley-VCH: Weinheim, 2007. (f) *Carbon-Rich Compounds: From Molecules to Materials*; Haley, M. M.; Tykwinski, R. R., Eds.; Wiley-VCH: Weinheim, 2006. (g) Thematic issue on "*Organic Electronics and Optoelectronics*": *Chem. Rev*. **2007**, *107 (4)*, 923–1386. (h) Thematic issue on "*Organic Photovoltaics*": *Acc. Chem. Res.* **2009**, *42 (11)*, 1689–1857. (i) Thematic issue on "*Materials for Electronics*": *Chem. Rev.* **2010**, *110 (1)*, 1–574. (j) Special issue on "*π-Functional Materials*": *Chem. Mater*. **2011**, *23 (3)*, 309–922.

(2) For applications in light-emitting diodes, see: (a) *Organic Light Emitting Devices: Synthesis, Properties and Applications*; Müllen, K.; Scherf, U., Eds.; Wiley-VCH: Weinheim, 2006. (b) Shirota, Y.; Kageyama, H. *Chem. Rev.* **2007***, 107*, 953–1010.

(3) For applications in photovoltaics, see: (a) Schmidt-Mende, L.; Fechtenkötter, A.; Müllen, K.; Moons, E.; Friend, R. H.; MacKenzie, J. D. *Science* **2001***, 293*, 1119-1122. (b) Walzer, K.; Maennig, B.; Pfeiffer, M.; Leo, K. *Chem. Rev.* **2007***, 107*, 1233–1271. (c) *Organic Photovoltaics: Materials, Device Physics, and Manufacturing Technologies*; Brabec, C.; Dyakonov, V.; Scherf, U., Eds.; Wiley-VCH: Weinheim, 2008. (d) Delgado, J. L.; Bouit, P.-A.; Filippone, S.; Herranz, M. A.; Martín, N. *Chem. Commun.* **2010***, 46*, 4853–4865. (e) Walker, B.; Kim, C.; Nguyen, T.-Q.

Chem. Mater. **2011***, 23*, 470–482.

(4) For applications in sensing, see: (a) Swager, T. M. *Acc. Chem. Res.* **1998***, 31*, 201–207. (b) McQuade, D. T.; Pullen, A. E.; Swager, T. M. *Chem. Rev.* **2000***, 100*, 2537–2574. (c) Thomas, S. W., III; Joly, G. D.; Swager, T. M. *Chem. Rev.* **2007***, 107*, 1339–1386. (d) Zang, L.; Che, Y.; Moore, J. S. *Acc. Chem. Res.* **2008***, 41*, 1596–1608.

(5) *Electronic Materials: The Oligomer Approach*; Müllen, K.; Wegner, G., Eds.; Wiley–VCH: New York, 1998.

(6) (a) Sandanayake, K. R. A. S.; Nakashima, K.; Shinkai, S. J. *Chem. Soc. Chem. Commun*. **1994**, 1621–1622. (b) McFarland, S. A.; Finney, N. S. *J. Am. Chem. Soc.* **2001***, 123*, 1260–1261. (c) McFarland, S. A.; Finney, N. S. *J. Am. Chem. Soc.* **2002***, 124*, 1178–1179. (d) Lee, D. H.; Im, J. H.; Lee, J.-H.; Hong, J.-I. *Tetrahedron Lett.* **2002***, 43*, 9637–9640. (e) Cody, J.; Fahrni, C. J. *Tetrahedron* **2004***, 60*, 11099–11107.

(7) Grimsdale, A. C.; Müllen, K. *Angew. Chem. Int. Ed.* **2005***, 44*, 5592–5629.

(8) Opsitnick, E.; Lee, D. *Chem. Eur. J*. **2007**, *13*, 7040–7049.

(9) (a) Young, J. K.; Moore, J. S. In *Modern Acetylene Chemistry*; Stang, P. J., Diederich, F., Eds.; VCH: Weinheim, Germany, 1995, pp 415–442. (b) Moore, J. S. *Acc. Chem. Res*. **1997**, *30*, 402–413. (c) Balzani, V.; Ceroni, P.; Maestri, M.; Vicinelli, V. *Curr. Opin. Chem. Biol.* **2003***, 7*, 657–665. (d) De Schryver, F. C.; Vosch, T.; Cotlet, M.; Van der Auweraer, M.; Müllen, K.; Hofkens, J. *Acc. Chem. Res.* **2005***, 38*, 514–522. (e) Lo, S.-C.; Burn, P. L. *Chem. Rev.* **2007***, 107*, 1097–1116. (f) Astruc, D.; Boisselier, E.; Ornelas, C. *Chem. Rev.* **2010***, 110*, 1857–1959.

(10) Jiang, X.; Bollinger, J. C.; Lee, D. *J. Am. Chem. Soc.* **2006***, 128*, 11732–11733.

(11) Lim, Y.-K.; Jiang, X.; Bollinger, J. C.; Lee, D. *J. Mater. Chem*. **2007**, *17*, 1969–1980.

(12) Jiang, X.; Vieweger, M. C.; Bollinger, J. C.; Dragnea, B.; Lee, D. *Org. Lett.* **2007***, 9*, 3579–3582.

(13) Riddle, J. A.; Jiang, X.; Huffman, J.; Lee, D. *Angew. Chem. Int. Ed.* **2007***, 46*, 7019–7022.

(14) Riddle, J. A.; Jiang, X.; Lee, D. *Analyst* **2008***, 133*, 417–422.

(15) Jiang, X.; Lim, Y.-K.; Zhang, B. J.; Opsitnick, E. A.; Baik, M.-H.; Lee, D. *J. Am. Chem. Soc.* **2008***,*

130, 16812–16822.

(16) (a) Chong, J. H.; Sauer, M.; Patrick, B. O.; MacLachlan, M. J. *Org. Lett.* **2003**, *5*, 3823–3826. (b) Sauer, M.; Yeung, C.; Chong, J. H.; Patrick, B. O.; MacLachlan, M. J. *J. Org. Chem.* **2006**, *71*, 775–788.

(17) (a) Yelamaggad, C. V.; Achalkumar, A. S.; Rao, D. S. S.; Prasad, S. K. *J. Am. Chem. Soc*. **2004**, *126*, 6506–6507. (b) Yelamaggad, C. V.; Achalkumar, A. S.; Rao, D. S. S.; Prasad, S. K. *J. Org. Chem.* **2007**, *72*, 8308–8318. (c) Yelamaggad, C. V.; Achalkumar, A. S.; Rao, D. S. S.; Prasad, S. K. *J. Mater. Chem.* **2007**, *17*, 4521–4529. (d) Yelamaggad, C. V.; Achalkumar, A. S.; Rao, D. S. S.; Prasad, S. K. *J. Org. Chem*. **2009**, *74*, 3168–3171.

(18) Riddle, J. A.; Lathrop, S. P.; Bollinger, J. C.; Lee, D. *J. Am. Chem. Soc.* **2006***, 128*, 10986–10987.

(19) Iskra, J.; Stavber, S.; Zupan, M. *Synthesis* **2004**, 1869–1873.

(20) Adams, M. J.; Highfield, J. G.; Kirkbright, G. F. *Anal. Chem.* **1980***, 52*, 1260–1264.

(21) Williams, A. T. R.; Winfield, S. A.; Miller, J. N. *Analyst* **1983**, *108*, 1067–1071.

(22) Beechem, J. M. *Methods Enzymol.* **1992***, 210*, 37–54.

(23) Beechem, J. M.; Ameloot, M.; Brand, L. *Chem. Phys. Lett.* **1985***, 120*, 466–472.

(24) Beechem, J. M.; Brand, L. *Photochem. Photobiol.* **1986***, 44*, 323–329.

(25) Boens, N.; Ameloot, M.; Valeur, B. *Springer Ser. Fluoresc.* **2008***, 5*, 215–232.

(26) Boens, N.; et al. *Anal. Chem*. **2007**, *79*, 2137–2149.

(27) Grinvald, A.; Steinberg, I. Z. *Anal. Biochem.* **1974***, 59*, 583–598.

(28) O'Connor, D. V.; Ware, W. R.; Andre, J. C. *J. Phys. Chem.* **1979***, 83*, 1333–1343.

(29) van Stokkum, I. H. M. In *IEEE Instrum. Meas. Technol. Conf. IMEKO Tech. Comm. 7* **1996**; Vol. 1, pp 168–173.

(30) Demas, J. N. *Excited state lifetime measurements*; Academic Press: New York, 1983.

(31) Sillen, A.; Engelborghs, Y. *Photochem. Photobiol*. **1998**, *67*, 475–486.

(32) Valeur, B. *Molecular Fluorescence: Principles and Applications*; Wiley-VCH: Weinheim, Germany, 2002.

(33) Lakowicz, J. R. *Principles of Fluorescence Spectroscopy*; 3rd ed.; Springer: New York, 2006.

(34) Loefroth, J. E. *J. Phys. Chem*. **1986**, *90*, 1160–1168.

(35) (a) Bushey, M. L.; Nguyen, T.-Q.; Nuckolls, C. *J. Am. Chem. Soc*. **2003**, *125*, 8264–8269. (b) Nguyen, T.-Q.; Martel, R.; Avouris, P.; Bushey, M. L.; Brus, L.; Nuckolls, C. *J. Am. Chem. Soc.* **2004***, 126*, 5234–5242. (c) Schenning, A. P. H. J.; van Herrikhuyzen, J.; Jonkheijm, P.; Chen, Z.; Würthner, F.; Meijer, E. W. *J. Am. Chem. Soc.* **2002***, 124*, 10252–10253. (d) Ajayaghosh, A.; Varghese, R.; Mahesh, S.; Praveen, V. K. *Angew. Chem. Int. Ed.* **2006***, 118*, 7729–7732. (e) Smulders, M. M. J.; Schenning, A. P. H. J.; Meijer, E. W. *J. Am. Chem. Soc.* **2008***, 130*, 606–611. (f) Nguyen, T.-Q.; Martel, R.; Bushey, M.; Avouris, P.; Carlsen, A.; Nuckolls, C.; Brus, L. *Phys. Chem. Chem. Phys.* **2007***, 9*, 1515–1532. (g) Hoeben, F. J. M.; Jonkheijm, P.; Meijer, E. W.; Schenning, A. P. H. J. *Chem. Rev.* **2005***, 105*, 1491–1546.

(36) Vargas, V. *J. Phys. Chem. A* **2004**, *108*, 281–288.

(37) Malar, E. J. P.; Jug, K. *J. Phys. Chem.* **1985***, 89*, 5235–5239.

(38) Amatatsu, Y.; Hosokawa, M. *J. Phys. Chem. A* **2004**, *108*, 10238–10244.

(39) Turro, N. J. *Modern Molecular Photochemistry*; University Science Books: Sausalito, CA, 1991.

(40) Friend, R. H.; Bradley, D. D. C.; Townsend, P. D. *J. Phys. D: Appl. Phys*. **1987**, *20*, 1367–1384.

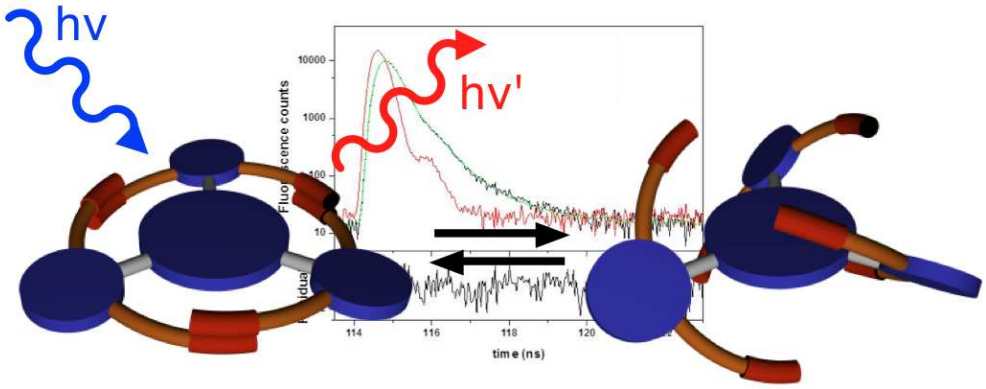

Correlated bond twisting motions reversibly switch the emission properties of C3-symmetric π-conjugation, the relaxation mechanisms of which were investigated by time-resolved spectroscopy.
88x34mm (300 x 300 DPI)